Colloid Polym Sci (2013) 291:2579–2587
DOI 10.1007/s00396-013-3004-z

ORIGINAL CONTRIBUTION

Sonochemical activation calcium sulfate whisker with enhanced beta-nucleating ability for isotactic polypropylene

Jun Qin · Wenjian Shi · Hongyan Yang · Jiang Liu · Jie Yu · Qing Lv · Yaozhu Tian

Received: 31 January 2013 / Revised: 21 May 2013 / Accepted: 5 June 2013 / Published online: 23 June 2013

Abstract The crystalline morphology, structure, and the β-nucleating ability of ultrasound-activated calcium sulfate whisker (CSW)-filled isotactic polypropylene were investigated via X-ray diffraction (XRD), polar light microscopy (PLM), and differential scanning calorimetry (DSC). The XRD results revealed that ultrasound treated CSW (UCSW) could improve the β-nucleated ability, and resulted in enhancing the content of β-crystal form. The ultrasonic time was conducive to the improvement of the contents of β-crystal and reached the maximum value at ultrasonic 120 min. PLM and DSC results verified the enhanced nucleating ability of UCSW supported as β-nucleating agent. The scanning electron microscopy, energy dispersive spectroscopy, Fourier transform infrared spectroscopy, and X-ray photoelectron spectroscopy indicated the surface of CSW treated by ultrasound had been changed. The activity of the calcium ion was improved and the sulfuric acid layer appeared on the whisker surface had a significant effect on the iPP β-heterogeneous nucleation, and resulted in enhancing the content of β-crystal form.

Keywords Polypropylene · Calcium sulfate whisker · Ultrasound · β-Crystalline form

J. Qin (✉) · W. Shi · J. Liu · Q. Lv
Key Laboratory of Karst Environment and Geohazard Prevention, Guizhou University, Ministry of Education, Guiyang 550003, China
e-mail: qi_njun@163.com

H. Yang · Y. Tian
The Material and Metallurgy College, Guizhou University, Guiyang 550003, China

J. Qin · J. Yu (✉)
National Engineering Research Center for Compounding and Modification of Polymer Materials, Guiyang, 550014, China
e-mail: yujiegz@126.com

Introduction

Isotactic polypropylene (iPP) is one of the most important semi-crystalline polymorphic materials with at least four basic crystalline forms: α (monoclinic), β (trigonal), γ (orthorhombic), and smectic forms [1–3]. Among these crystalline forms, due to excellent thermal, mechanical properties (especially impact resistance), and fine elongation at break, β-nucleated iPP has aroused widely attention between scientific research and industrial applications [4–9]. However, the β-crystal form is difficult to obtain due to thermodynamical metastability under normal processing conditions. There are three methods to improve the β-crystalline form: adding heterogeneous nucleating agents [10–18], shear-induced crystallization [19–25] and temperature gradients method [26]. Of which, the most effective and practical method to obtain the iPP with the higher β crystal content is the adding of so-called β-nucleating agents [10–18, 27].

Until now, there are only four classes of compounds used as β-nucleating agents: organic pigment compounds; amorphous polymeric nucleating agents such as styrene acrylonitrile and polystyrene [14, 15]; aromatic amide compounds include 1,3,5-benzenetrisamides[27], aryl amide derivative (TMB-5) [16], and N, N′-dicyclohexy-2, 6-naphthalenedicarboxamide (NJ Star) [17]; IIA metal salts; or their mixtures with some specific dicarboxylic acids [18]. Among these β-nucleating agents, inorganic nucleated agents, due to their lower nucleating effect and higher loading, are frequently neglected. Liu et al. added 17.7 % (volume ratio) wollastonite in the PP, only getting 37 % β crystal form of PP [28]. At the carbonate/PP system, even if the adding load of carbonate reached 40 %, the β crystal form PP was only 12 % [29]. Therefore, adopting a new method, to improve the nucleating effect of the nucleated inorganic agents to get better stiffness and toughness and thermal properties simultaneously is very meaningful. Recently, calcium sulfate whisker (CSW) has attracted a great number

of interests and been widely studied due to its almost perfect crystal structure, low cost, chemical resistance, and possessing high strength and stiffness [30]. In this study, ultrasound-treated CSW (UCSW) to enhance iPP β-nucleating ability for getting better mechanical and thermal properties is investigated.

To the authors' knowledge, UCSW as a reinforcing phase and β-nucleating agent in polymeric materials has never been reported until now. The novelty of this article is that UCSW improving the β-nucleating ability of iPP was prepared. The influence of UCSW on the β-nucleating ability of iPP had been investigated via X-ray diffraction (XRD) and differential scanning calorimeter (DSC), respectively. Moreover, the structure of CSW/iPP and UCSW/iPP composites was researched by polarized light microscopy (PLM). In addition, the surface changes of UCSW were also discussed with scanning electron microscopy (SEM), energy dispersive spectroscopy (EDS), Fourier transform infrared spectroscopy (FTIR), and X-ray photoelectron spectroscopy (XPS).

Experimental materials and methods

Materials

CSW was synthetized by the hydrothermal method in our lab, the formula was $CaSO_4{\cdot}2H_2O$. Polypropylene was kindly supplied by Lanzhou Petroleum and Chemistry Co.,Ltd. (Lanzhou, China), with $M_w=10.6\times10^4$ g/mol and $M_w/M_n=3.5$, and was adopted as basal resin. Ethanol, analytical pure, was supported by Chuanjiang Chemical Reagent Factory (Chongqing, China). UCSW was prepared as follows: 100 g of CSW were gradually added to 1 l ethanol solution, vibrated about 40–200 min in the ultrasonic generator, filtered, and dried in a vacuum oven at 50°C for 12 h, and then finely ground.

Preparations of UCSW/PP and CSW/iPP composites

The iPP granules and UCSW or CSW (the mass ratio of iPP: UCSW or CSW=85:15) were mixed in a high-speed mixer for 10 min, and were extruded in a two-screw extruder (Type TSSK-3540, Zhangjiagang, China) to form masterbatches. The screw speed was fixed at 300 rpm. Then, in an injection molding machine (Type PL860/290 V, Wuxi, China), different masterbatches were further melted to prepare UCSW or CSW/iPP composites. The processing temperature was 170~210 °C from hopper to nozzle.

Characterizations and measurements

SUNNY XP-P (NingBo, China) polarized light microscopy attached with a Canon Power Shot G10 digital camera and a KER3100-08S hot-stage (NanJing, China) were generally used to investigate the morphology of pure iPP, CSW-, and UCSW-filled iPP. The extruded samples were placed in microscopy slides, melted, and pressed at 190 °C for 5 min to erase any trace of crystal, and then rapidly cooled to a predetermined crystallization temperature (124 °C). The samples were kept isothermal until the crystallization process was completed, and photographs were automatically taken simultaneously.

DSC (AQ20, USA) was carried out to measure the β-form content and study the crystallization peak temperature. Temperature was calibrated by using indium as a standard medium before the measurements. About 5 mg of sample was weighed accurately before each run. The samples measurements were performed at a standard heating and cooling rate of 10 °C min^{-1} under nitrogen atmosphere. Starting from 40 to 190 °C and the samples were held up to 190 °C for 5 min to erase the thermal and mechanical history, first cooled to 40 °C and melting to 190 °C for 5 min to record crystallization and melting curves, then cooled to 124 °C for isothermal crystallization for 10 min and directly heated to 190 °C to record crystallization and melting curves in order to avoid the possible transformation from β-iPP to α-iPP during the melting process [31–33], the relative content of β form could be calculated correctly.

The degree of crystallization [16] was calculated as follow:

$$X_i = \frac{\Delta H_i}{\Delta H_i^0} \times 100\% \tag{1}$$

Where ΔH_i is the calibrated specific enthalpy of fusion of either α or β form, and ΔH_i^0 is the standard enthalpy of fusion of either α or β form, 177 J/g for α form and 168.5 J/g for β form. The ΔH_i of overlapping of α- and β-form peaks were determined according to Li et al. calibration method [34]. X_i is the crystallinity of α form and β form, respectively. The relative content of β form could be calculated by the following equation:

$$\phi_\beta = \frac{X_\beta}{X_\alpha + X_\beta} \times 100\% \tag{2}$$

The specimens for XRD were cut into 0.4 mm thick and performed using a PANalytical X'Pert diffractometer (PANalytical, Netherlands), in a reflection mode using Cu-Kα radiation under a current of 40 mA and a voltage of 40 kV. The speed of scanning was 0.334°/s and diffraction angle 2θ was recorded in the region of 5–60°. The X-ray curves were constituted with crystallinity and amorphous peaks. The overall crystallinity X_c was calculated by Huo et al. [24]:

$$X_c = \left(1 - \frac{\sum A_{\text{amorphous}}}{\sum A_{\text{crystallization}} + \sum A_{\text{amorphous}}}\right) / (1 - m_c/(m_c + m_{\text{iPP}})) \tag{3}$$

Where $A_{\text{crystallization}}$ and $A_{\text{amorphous}}$ are the areas of the crystallization and amorphous peak, respectively; m_c and m_{iPP} are

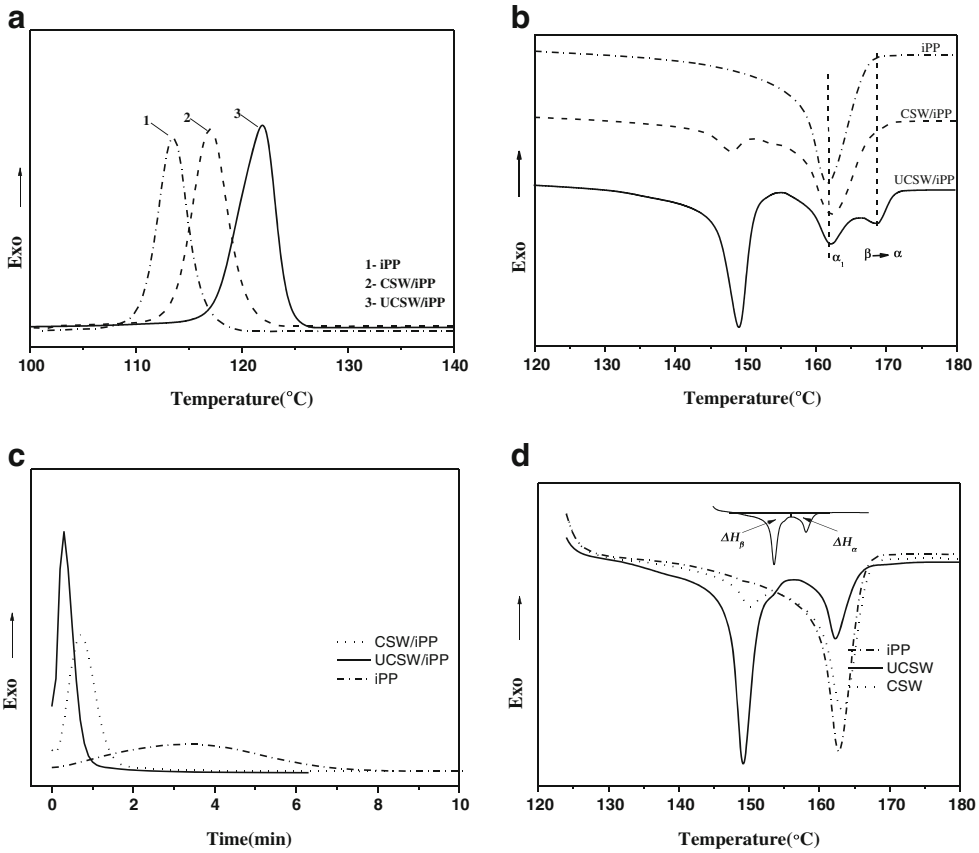

Fig. 1 DSC crystallization (**a**, **c**) and melting curves(**b**, **d**) of iPP blend with CSW and UCSW: **a** crystallized from 40–190 °C by 10 °C/min; **b** melting from 40–190 °C; **c** crystallized at 124 °C 10 min; **d** directly melting form 124–190 °C

the mass of the calcium sulfate whisker and the pure iPP, respectively. The relative amount of the β crystal form K_β, the relative crystalline degree of the β crystal form X_β and the relative crystalline degree of the α crystal form X_α are determined according to the standard procedures described in the literature [35], which are given by:

$$K_\beta = \frac{A_\beta(300)}{A_\alpha(110) + A_\alpha(040) + A_\alpha(130) + A_\beta(300)} \quad (4)$$

$$X_\beta = K_\beta \times X_c \quad (5)$$

$$X_\alpha = 1 - K_\beta \times X_c \quad (6)$$

Where A_Ω (h k l) denotes the intensity of the respective (h k l) peak, A_β (300) is the area of the (300) reflection peak; A_α (110), A_α (040), and A_α (130) are the areas of the (110), (040), and (130) reflection peaks, respectively.

SEM analysis was performed with a JSM-6490LV scanning electron microscope on cryogenically fractured samples at 20 kV. The element content on the surface of CSW was calculated using data determined by an EDS-2100 system.

The FTIR of the CSW and UCSW was obtained using a Nicolet NEXUS-670 FTIR spectrometer.

Surface compositions were measured by XPS on an XSAM800 spectrometer (Kratos Analytical Ltd., Manchester, Lancashire, UK) with a monochromatic Al KR X-ray source (1,486.6-eV photons) at a constant dwell time of 100 ms and a pass energy of 40 eV. The anode voltage was 15 kV, and the anode current was 10 mA, the pressure was maintained at 7.0×10^{-6} Pa or lower during each measurement in the analysis chamber. The core-level signals were obtained at a photoelectron takeoff angle of 90° (with respect to the sample surface), and all binding energies (BEs) were referenced to the C 1-s hydrocarbon peak at 284.6 eV. Surface elemental stoichiometries were determined from XPS spectral area ratios and were reliable to within ±5%.

Table 1 Parameters of pure iPP and calcium sulfate whisker/iPP composites

Sample	T_p (°C)	T_m for iPP (°C)		ΔH_m for iPP (J/g)		Φ_β	Origin
		α	β	α	β		
iPP	113.47	160.44	–	72.75	–	–	(b)
	–	162.82	–	85.92	–	–	(d)
CSW/iPP	117.07	160.96	146.83	61.88	12.68	17.71	(b)–β→α
	–	163.26	150.11	59.97	22.76	28.50	(d)
UCSW/iPP	121.97	162.27	149.18	30.86	48.36	62.20	(b)–β→α
	–	162.17	149.13	5.60	63.14	92.21	(d)

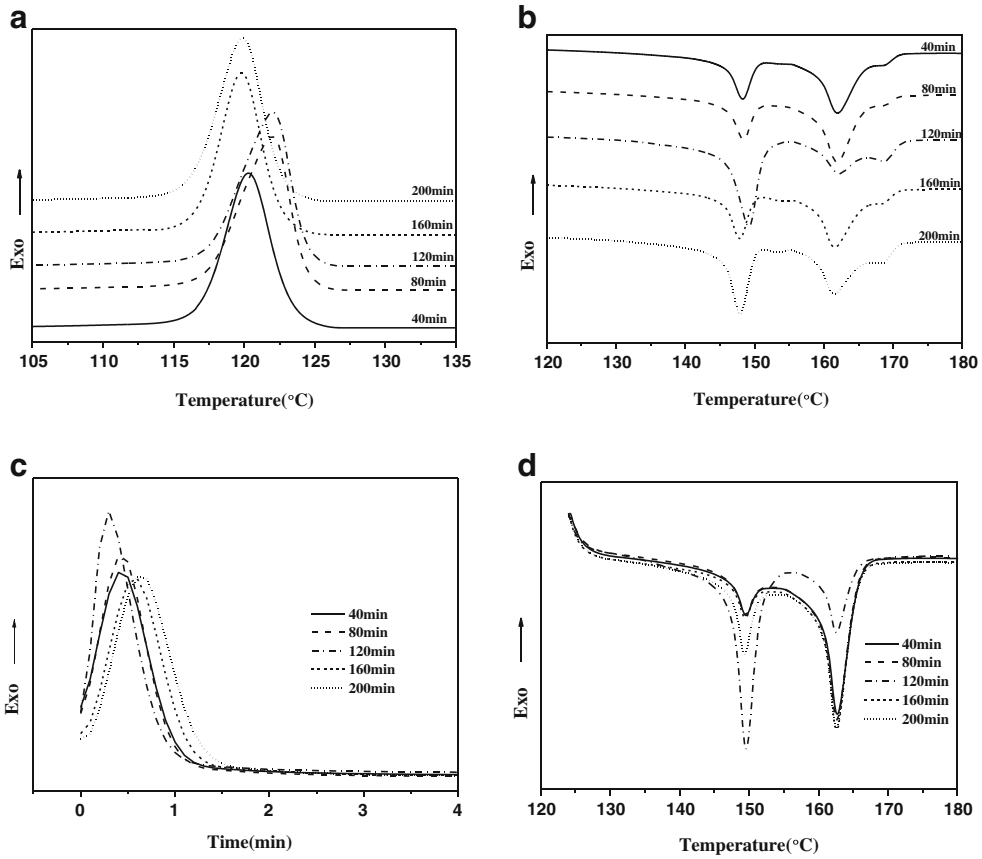

Fig. 2 DSC crystallization (**a**, **c**) and melting curves(**b**, **d**) of iPP nucleated by UCSW treated at different ultrasonic time: **a** crystallized from 40 to 190 °C by 10 °C/min; **b** melting from 40 to 90 °C; **c** crystallized at 124 °C 10 min; **d** directly melting form 124 to 190 °C

Results and discussion

The β-nucleating ability of UCSW

Figure 1 shows the DSC crystallization and melting curves of iPP and iPP blend with CSW and UCSW respectively. According to Eqs. 1 and 2, the crystallization and melting parameters were calculated and listed in Table 1. Figure 1b also indicates that the transformation of PP phases among UCSW/iPP from β-iPP to α-iPP exists during the melting process [31–33] because the samples were cooled below the critical (TR) temperature. Figure 1d indicates that there is not the transformation of UCSW/iPP from β-iPP to α-iPP during the melting process because the samples were cooled higher than the critical (TR) temperature and the disturbing effect of β- to α-recrystallization had been eliminated. This method is used for exact characterization of the efficiency and selectivity of CSW or UCSW.

As shown in Fig. 1 and Table 1, CSW/iPP and UCSW/iPP composites exhibit two melting peaks, $T_{m\alpha}$ and $T_{m\beta}$, corresponding to the α- and β-crystals, respectively, suggesting that CSW can induce iPP to produce β-crystal form slightly and UCSW cause iPP to generate more β-crystal form, increasing the content of β-crystal form from 28.50 to 92.21%, triple more than its initiatives in CSW/iPP composites. Adding CSW and UCSW can increase crystallization temperature of iPP as shown as Fig. 1a, and for the pure iPP, the temperature of crystallization peak is 113.47 °C. The incorporation of 15 wt% of CSW in isotactic polypropylene produced a slight shift of crystallization peak toward a higher temperature 117.07 °C, while the T_p of UCSW/iPP shift to 121.97 °C,

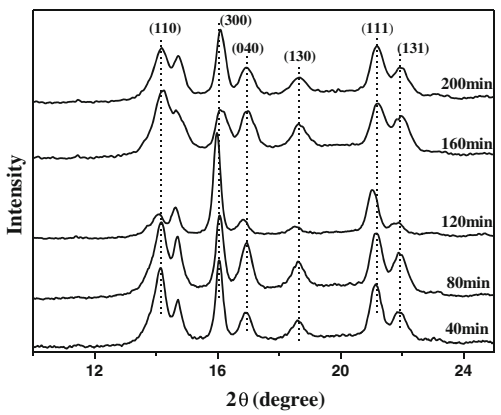

Fig. 3 XRD of iPP nucleated by UCSW treated at different ultrasonic time

Table 2 Parameters of crystallizaton for pure iPP and UCSW-nucleated PP composites at different ultrasonic time

Sample	T_{co} (°C)	T_{cp} (°C)	T_m for PP (°C)		ΔH_m for PP (J/g)		Φ_β	K_β	Origin
			α	β	α	β			
40 min	123.33	120.32	162.00	148.25	47.76	24.35	34.90	0.34	(b)–β→
	–	–	162.76	149.57	22.96	53.01	31.27		(d)
80 min	123.69	120.89	161.90	148.39	51.28	23.59	32.58	0.30	(b)–β→
	–	–	162.64	149.45	22.41	54.23	30.27		(d)
120 min	124.32	121.97	162.27	149.18	30.86	48.36	62.20	0.72	(b)–β→
	–	–	162.17	149.13	5.60	63.14	92.21		(d)
160 min	122.55	119.79	161.56	147.83	47.50	23.05	33.76	0.24	(b)–β→
	–	–	162.65	149.47	21.84	54.79	29.51		(d)
200 min	122.66	119.89	161.55	147.95	47.02	33.79	43.03	0.41	(b)–β→
	–	–	162.50	149.42	31.79	52.48	37.72		(d)

which is the highest crystallization peak temperature among these samples. The CSW processing by ultrasound had a higher effect of the heterogeneous nucleation to iPP, which may enhance the content of β-crystal form and improve crystallization rate of iPP obviously as shown as Fig. 1c.

Ultrasonic time

Figure 2 indicates the DSC crystallization and melting curves, and Fig. 3 shows the XRD of iPP nucleated with UCSW was treated by different ultrasonic time. The crystallization and

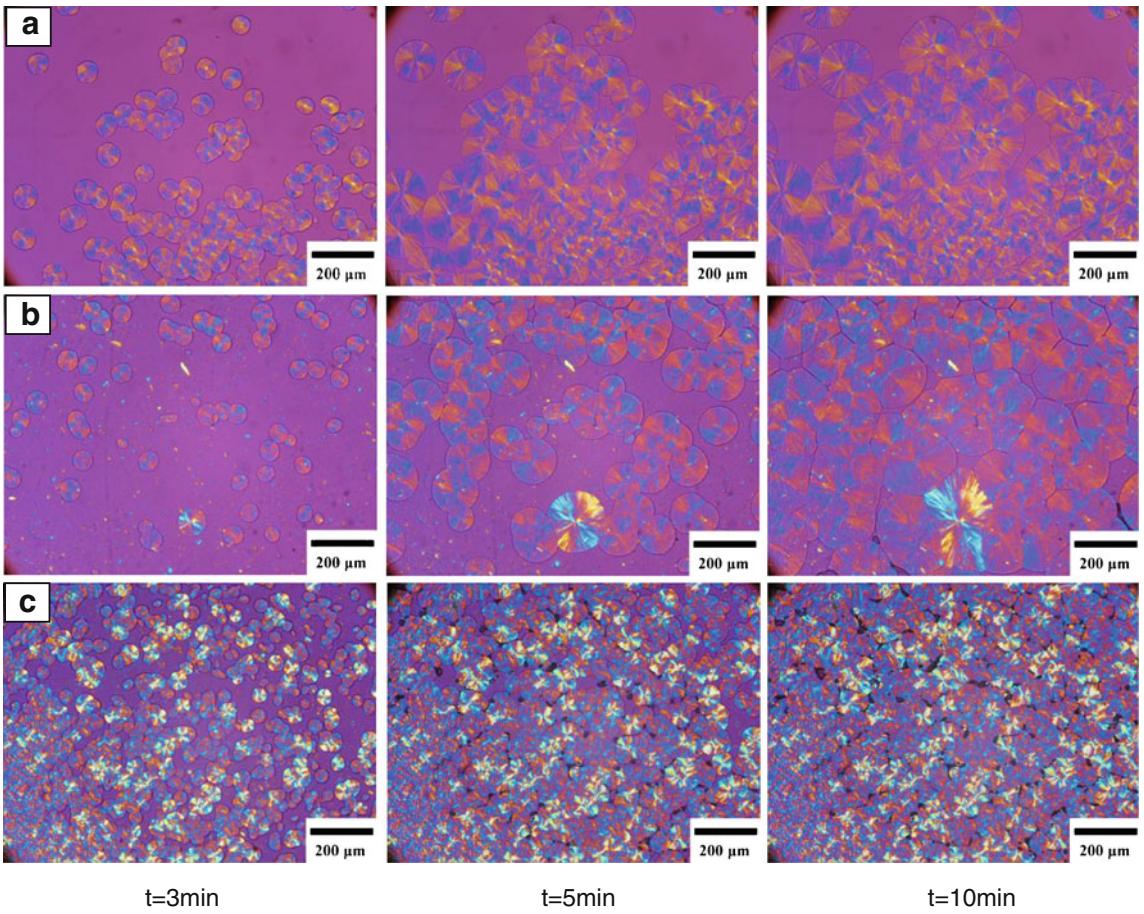

Fig. 4 Spherulite morphology of iPP composites under different crystallization times crystallized at 124 °C, magnification ×100 (*bar*: 200 μm): **a** pure iPP; **b** iPP/CSW and **c** iPP/UCSW composites

melting parameters of Figs. 1, 2 and 3 according to Eqs. 1–6 are listed in Table 2. It can be seen clearly from Fig. 3 that these common characteristic diffraction angles at 2θ angles of 14.0°, 16.8°, 18.6°, 21.2°, and 21.9° appeared in all samplers, are corresponding to the (110), (040), (130), (111), and (131) reflections of iPP α-monoclinic crystal, and indicates iPP α-crystal form existing. The peak appears at 2θ angles of about 16.0° is corresponding to the (300) reflection of the hexagonal iPP β-crystal form. The (200) and (020) reflections appears at 2θ angles of about 14.7° and 25.6° are corresponding to the characteristic peaks of semihydrate calcium sulfate whisker(τ form of CSW, which has hexagonal configuration with a=0.699nm and c=0.634nm). These reflections indicate that the crystal of the CSW is transformed to the τ form of CSW after dehydrating; the τ CSW may be one important factor increasing the β-nucleating ability, which in turn nucleates preferentially the β-crytal form of PP at 115°C [36]. With the increase of the intensity ration of the (200) and (020) reflections of τ CSW to the (300) reflection of the hexagonal iPP β-crystal form, the β-crystal content were enhanced, indicating the more τ CSW produced in polymer processing is helpful to form the β-crystal in iPP sample. However, how to control the generation of τ CSW would be a worth further research topic.

It can be obviously seen that T_{cp} and the content of β-crystal of iPP increases until the ultrasonic time reaches 120 min, the maximum value of β-crystal form up to 62.20 % for DSC, and 72.46 %for XRD (the crystallinity calculated from the XRD analyses listed in Table 2) were received. These results assuredly indicate that CSW by ultrasound can induce iPP to produce β-crystal efficiently. It can be explained that the surface of calcium sulfate whisker under the processing of ultrasound: as demonstrated by EDS and SEM, as shown below, the improved calcium ion activity and the cavity on the CSW surface appeared and the morphology changed; these results are advantageous to the adsorption of iPP on the CSW surface and enhancing the β-nucleating effect; at same time, those changes contributed to form τ CSW in the polymer processing. However, with the increasing of ultrasonic times, the τ CSW formation were destroyed, resulting in the decreasing the β-crystal form of iPP as shown as Figs.2 and 3 and Table 2.

Crystalline morphology

The XRD and DSC results indicate the calcium sulfate whisker processing by the ultrasound has nucleated heterogeneous effects resulting in the enhancement of the β-crystal form content of iPP. PLM also reveals that with the aid of UCSW supported as β-nucleating agent, the large majority of active nucleation sites are shaped, as shown in Fig. 4.

The morphology of pure iPP exhibiting large and perfect spherulites has a diameter of about 100 μm and no β-spherulites appearing after 10 min at 124 °C, as shown in Fig. 4a. When the isothermal crystallization temperature stabilized at 124 °C and for about 3 min, adding CSW makes few β-nuclei to appear, as shown in Fig. 4b. Although the

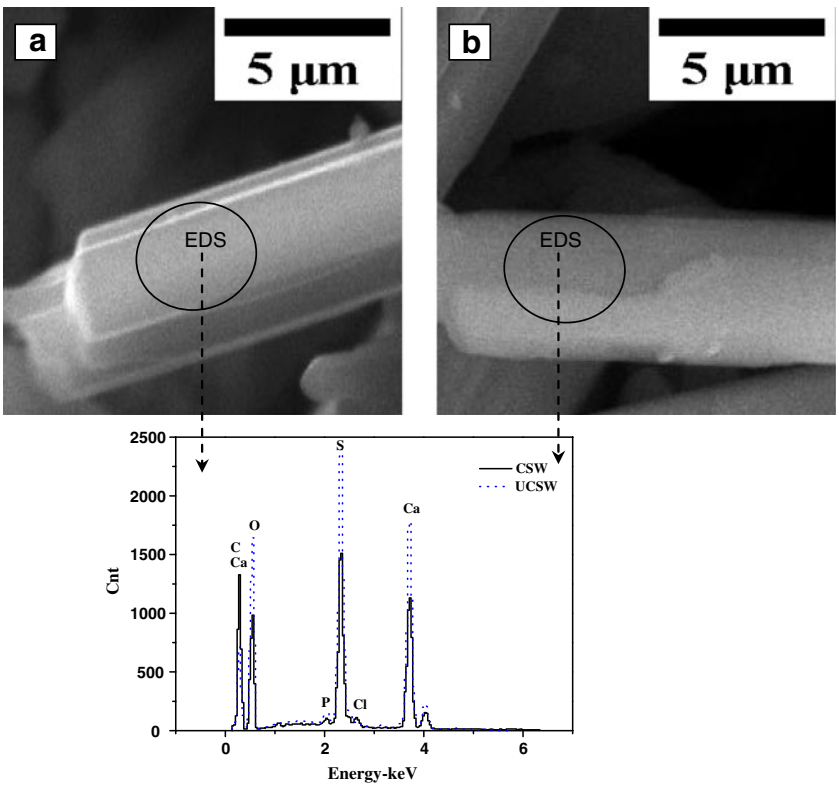

Fig. 5 The SEM and EDS graph of the CSW (**a**) and UCSW (**b**)

Table 3 Parameters of EDS analysis the surface of calcium sulfate whisker

Sample	Element (%)				
	O	S	Ca	P	Cl
CSW	68.84	13.81	15.92	0.42	1.01
UCSW	69.20	15.00	15.40	0.38	–

CSW has certain β-nucleated ability, few bright β-crystal forms appear, and the spherulite size of iPP nucleated with calcium sulfate whisker composites is almost unchanged, compared with that of α-crystal form as shown in Fig. 4a. When adding UCSW into iPP, the large number of β-crystal appeared after 3 min, indicating that the UCSW plays a novel and effective role of β-nucleating agent, and which not only reduces the spherulite size of iPP, but also increases the crystallization rate of iPP, as shown in Fig. 4c. The boundary of the β-crystal form is quite vague compared with that of α-crystal form. The morphological characteristics and crystallization process exhibit significant change after UCSW is incorporated into iPP. The UCSW-nucleated iPP shows more irregular spherulites and their boundaries are difficult to be distinguished, and the spherulites present a rod-like structure grown at the early stage of crystallization.

Surface characteristics

The SEM and EDS analysis

Figure 5 shows the SEM and EDS graph of the CSW and CSW treated by ultrasound (UCSW). The EDS analysis shows that after the CSW were dealt with ultrasound, the O concentration increased a little, and the S concentration increased, while the Cl concentration and P concentration decreased simultaneously, as shown in Table 3. Due to the impact of ultrasound (the density of ultrasonic power was about 0.35W/cm^2), surface cracks appeared on the smooth surface of CSW, resulting in the rough surface of UCSW with a lot of cavities; at the same time, a "calcium oxide or sulfuric acid layer" was gradually developed due to the action of hydrogen radicals [37, 38]. We hypothesize that because of these cavities and surfaces change, the β-nucleated capability of the iPP increases as shown in Fig. 6.

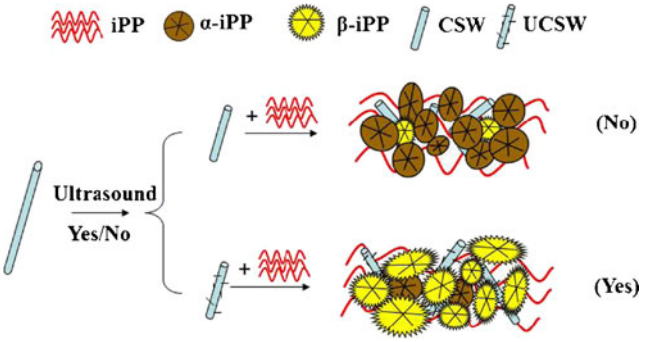

Fig. 6 Schematic crystallization processes of CSW- and UCSW-nucleated iPP

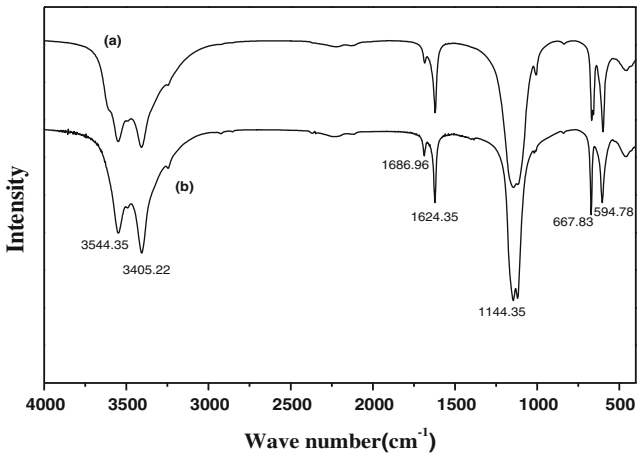

Fig. 7 The FTIR of CSW (**a**) and UCSW (**b**)

The FTIR analysis

Figure 7 shows the FTIR spectrum of CSW and UCSW. At 3,405 and 3,544 cm^{-1} are the OH group stretching vibrations. The former was produced by the hydroxylation of the calcium ion on the surface of the CSW; the latter was formed by the crystal water in the whisker internal. In the 1,624.35 and 1,686.96 cm^{-1} appear the OH group asymmetrical stretching vibration peaks, while at 1,144.35, 667.83, and 594.78 cm^{-1} emerge the $-SO_4$ absorption peaks. It is obvious that the OH group stretching vibration of UCSW is higher than that of CSW, suggesting that the CSW have

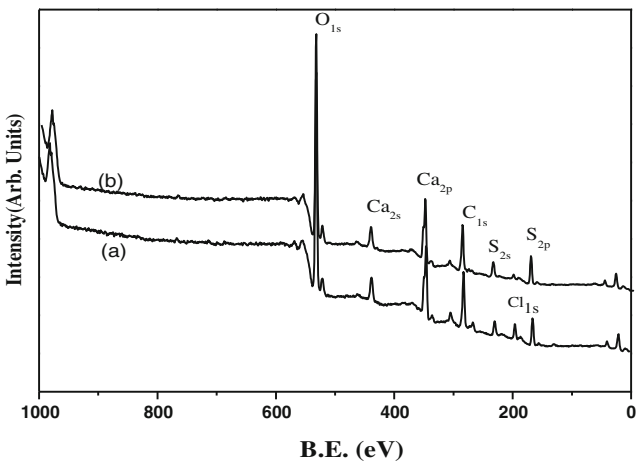

Fig. 8 The wide scan spectra of (**a**) CSW and (**b**) UCSW

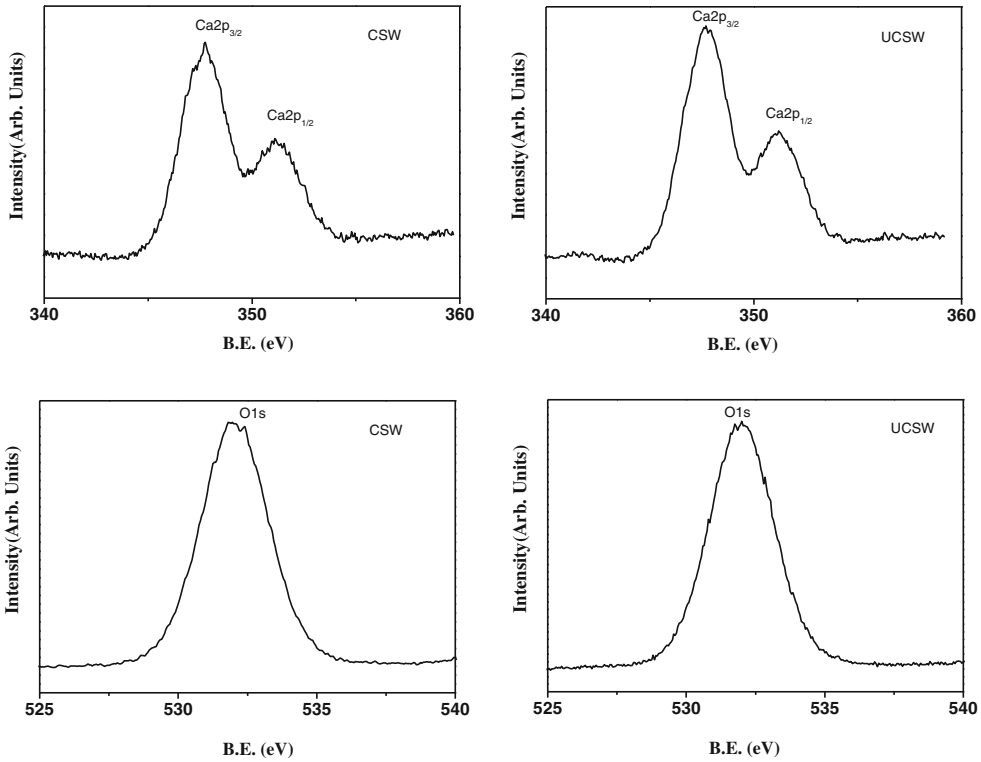

Fig. 9 The Ca_{2p} and O_{1s} core-level spectrum of the CSW and UCSW surface

hydration reaction partly under ultrasound and water molecules come into the whisker interior to form the crystal water. Compared with the strength produced by the hydroxylation of the calcium ion on the whisker surface at 3,405 cm^{-1}, the vibration peaks of UCSW is higher than that of CSW, suggesting that ultrasound is helpful to improve the activity of the calcium ion.

The XPS analysis

Figure 8 shows the wide scan spectra of CSW and UCSW. Figure 9 shows the Ca_{2p} and O_{1s} core-level spectrum of the CSW and UCSW surface, and the element percent of O, S, Ca, P, and Cl calculated according to Figs. 8 and 9 are listed in Table 4. The O_{1s} binding energies of CSW (532.40 eV) and UCSW surface are higher than the binding energy (532 eV) of calcium sulfate O_{1s}, but is lower than water's O_{1s} binding energy(532.8 eV), suggesting that the CSW and UCSW(532.83 eV) surface can absorb water physically and that there are OH groups on the surface; compared with $Ca2p_{3/2}$ binding energy(347.75 eV) of the CSW surface, the $Ca2p_{3/2}$ binding energies of UCSW surface have shifted to the lower-energy direction, and their deviants were 0.08 eV, indicating that hydroxylation reaction occurred on the whisker surface calcium ion more intensively, and the UCSW surface owned more protonation surface position >CaOH [39]. The XPS results also indicate that the O concentration was improved a little, while the S concentration increased, the Cl and P concentration decreased simultaneously. This also shows that the activity of the CSW surface calcium ion has been improved by the ultrasound, and is helpful to absorb iPP to form β-crystal.

Table 4 Parameters of XPS analysis the surface of calcium sulfate whisker

Sample	Element (%)				
	O	S	Ca	P	Cl
CSW	68.40	11.24	13.87	2.13	4.36
UCSW	69.97	13.21	13.44	1.96	1.42

Conclusions

Sonochemical activation calcium sulfate whisker to enhance isotactic polypropylene β-nucleating ability and influence on the crystal morphology, structure, and capability of nucleation were investigated in the current work. XRD and DSC results showed that CSW under the ultrasonic vibration was in favor to induce iPP to develop β-crystal, and gained the highest content of β-crystal form at the optimum ultrasonic time (120 min). XRD and DSC results were in keeping with the PLM investigation. It also revealed that with the aid of UCSW supported as β-nucleating agent, large majority of active nucleation sites were shaped and crystallized at 124 °C. The SEM, EDS, FTIR, and XPS indicated that the surface of CSW treated by ultrasound had been changed. The activity of

calcium ion has been improved and the sulfuric acid layer appeared on the whisker surface had a significant effect on the iPP β-heterogeneous nucleation, and resulted in enhancing the content of β-crystal form. Meanwhile, compared with that of α-crystal form and the β-crystal form in the iPP or CSW composites, the spherulite size of iPP nucleated with UCSW composites was decreased significantly; the presence of UCSW observably changed the crystal morphological characteristics and crystallization process, respectively.

Acknowledgments We would like to express our sincere thanks to the Natural Science Foundation of China for financial support (grant no. 21266005).

References

1. Lotz B, Wittmann JC, Lovinger AJ (1996) Polymer 37:4979–92
2. Varga J (1995) Crystallization, melting and supermolecular structure of isotactic polypropylene. In: Karger-Kocsis J (ed) Polypropylene: structure, blends and composites. Vol I. Structure and morphology, Ch 3. Chapman & Hall, London, pp 56–115
3. Varga J (2002) J Macromol Sci Phys B 41:1121–1171
4. Tjong SC, Shen JS, Li RKY (1995) Scr Met Mater 33:503–508
5. Karger-Kocsis J, Varga J, Ehrenstein GW (1997) J Appl Polym Sci 64:2057–2066
6. Karger-Kocsis J, Varga J (1996) J Appl Polym Sci 62:291–300
7. Tjong SC, Shen JS, Li RKY (1996) Polymer 37:2309–2316
8. Karger-Kocsis J, Mouzakis DE, Ehrenstein GW, Varga J (1999) J Appl Polym Sci 73:1205–1214
9. Varga J, Ehrenstein GW, Schlarb AK (2008) Express Polym Lett 2:148–156
10. Zeng AR, Zheng YY, Qiu SC, Guo Y, Li BM (2011) Colloid Polym Sci 289:1157–1166
11. Varga J, Mudra I, Gottfried W (1999) J Appl Polym Sci 74:2357–2368
12. Mathieu C, Thierry A, Wittmann JC, Lotz B (2002) J Polym Sci Part B Polym Phys 40:2504–2515
13. Mohmeyer N, Schmidt HW, Kristiansen PM, Altstädt V (2006) Macromolecules 39:5760–5767
14. Su ZQ, Dong M, Guo ZX, Yu J (2007) Macromolecules 40:4217–4224
15. Phillips A, Zhu PW, Edward G (2010) Polymer 51:1599–1607
16. Xiao WC, Wu PY, Feng JC (2008) J Appl Polym Sci 108:3370–3379
17. Varga J, Menyhárd A (2007) Macromolecules 40:2422–2431
18. Shi GY, Huang B, Zhang JY (1984) Makromol Chem Rapid Commun 5:573–578
19. Zhu PW, Edward G (2003) Macromol Mater Eng 288:301–311
20. Somani RH, Hsiao BS, Nogales A (2001) Macromolecules 34:5902–5909
21. Somani RH, Hsiao BS, Nogales A (2000) Macromolecules 33:9385–9394
22. Stocker W, Schumacher M, Graff S, Thierry A, Wittmann JC, Lotz B (1998) Macromolecules 31:807–814
23. Zipper P, Jánosi A, Wrentschur E, Abuja PM, Knabl C (1993) Prog Colloid Polym Sci 93:377–378
24. Huo H, Jiang SC, An LJ (2004) Macromolecules 37:2478–2483
25. Varga J, Karger-Kocsis J (1996) J Polym Sci Part B Polym Phys 34:657–670
26. Pawlak A, Piorkowska E (2001) Colloid Polym Sci 279:939–946
27. Blomenhofer M, Ganzleben S, Hanft D, Schmidt HW (2005) Macromolecules 38:3688–3695
28. Li JX, Cheung WL (2000) J Therm Anal Calorim 61:757–62
29. McGenity PM, Hooper JJ, Paynter CD, Riley AM, Nutbeem C, Elton NJ, Adams JM (1992) Polymer 33:5215–5224
30. Ong XF, Zhang LN, Zhao JC, Xu YX, Sun Z, Li P, Yu JG (2011) Cryst Res Technol 46:166–172
31. Varga J (1989) Therma Anal 35:1891–1912
32. Varga J (1986) Therma Anal 31:165–172
33. Varga J, Garzó G, IIIe A (1986) Angew Makromol Chem 142:171–181
34. Liu JJ, Wei XF, Guo QP (1990) J Appl Polym Sci 41:2829–2835
35. Turner JA, Aizlewood JM, Beckett DR (1964) Makromol Chem 75:134–154
36. Radhakrishnan S, Saujanya C (1998) J Mater Sci 33:1069–1074
37. Shchukin DG, Skorb E, Belova V, Möhwald H (2011) Adv Mater 23:1922–1934
38. Pai MR, Hassan PA, Bharadwaj SR, Kulshreshtha SK (2008) New J Chem 32:353–357
39. Stipp SL, Hochella MFJR, Parks GA, Leckie JO (1992) Geochim Cosmochim Acta 56:1941–1954